ARCHIVIO ISTITUZIONALE
DELLA RICERCA

Alma Mater Studiorum Università di Bologna
Archivio istituzionale della ricerca

Error vector magnitude measurement for power amplifiers under wideband load impedance mismatch: System-level analysis and VNA-based implementation

This is the final peer-reviewed author's accepted manuscript (postprint) of the following publication:

Published Version:
Gibiino G.P., Angelotti A.M., Santarelli A., Traverso P.A. (2022). Error vector magnitude measurement for power amplifiers under wideband load impedance mismatch: System-level analysis and VNA-based implementation. MEASUREMENT, 187, 1-10 [10.1016/j.measurement.2021.110254].

Availability:
This version is available at: https://hdl.handle.net/11585/841316 since: 2021-12-10

Published:
DOI: http://doi.org/10.1016/j.measurement.2021.110254

Terms of use:

Some rights reserved. The terms and conditions for the reuse of this version of the manuscript are specified in the publishing policy. For all terms of use and more information see the publisher's website.

This item was downloaded from IRIS Università di Bologna (https://cris.unibo.it/).
When citing, please refer to the published version.

(Article begins on next page)

09 January 2025

Error Vector Magnitude Measurement for Power Amplifiers under Wideband Load Impedance Mismatch: System-Level Analysis and VNA-based Implementation

Abstract

The Error Vector Magnitude (EVM) is a fundamental metric used in communications to quantify the wideband distortion generated by a non-linear system subject to modulated excitation. While typically adopted for impedance-matched devices, the EVM is here investigated for the performance assessment of mismatched power amplifiers (PAs) across wide modulation bandwidths (BWs). A system-level analysis is developed to characterize the EVM for a non-linear device cascaded with a generic linear network. To study particular operating regimes of interest under wideband load mismatch, the EVM measurement process is here applied together with a novel wideband active load-pull technique, leading to a newly implemented frequency-domain characterization platform based on classical relative measurements from a Vector Network Analyzer (VNA). The experimental results ultimately show that the analyzed EVM measurement method can be consistently and effectively combined with load-pull techniques in realistic application cases, enabling improved wideband radio-frequency (RF) PA design and characterization.

Keywords: error vector magnitude, modulation distortion, wideband measurements, load-pull, power amplifiers.

1. Introduction

As communication systems are evolving to higher data rates, signal modulations feature even wider modulation bandwidths (BWs). Correspondingly, the performance of electron devices and sub-systems within the transmitter/receiver

modules must be properly characterized by suitable wideband metrics [1]. Indeed, orthogonal frequency-division multiplexing (OFDM) schemes featuring high data-rate modulations can effectively be employed only if sufficient signal quality is achieved across the full communication chain. In this sense, the most critical devices within the radio-frequency (RF) systems are the non-linear ones, particularly power amplifiers (PAs) and mixers.

Whereas classical experimental frameworks for characterizing the non-linear behaviour of a Device-Under-Test (DUT) are based on continuous-wave (CW), pulsed-CW, or two-tone excitations [2, 3, 4, 5, 6, 7], only test signals resembling the actual application-like operating regimes, e.g., complex modulation test waveforms or suitably designed multi-tone signals [8, 9, 10], are truly reliable for the characterization of DUTs to be operated under wideband operating regimes. These normally require baseband signal synthesis of the in-phase/quadrature (IQ) components by means of an Arbitrary Waveform Generator (AWG) and up-conversion by an IQ-mixer in a Vector Signal Generator (VSG) architecture [11], while the measurement of the envelope waveform at the DUT output is performed through wideband IQ down-conversion and subsequent demodulation by a Vector Signal Analyzer (VSA). In the typical set-up implementation (Fig. 1a), the mixers are fed by the same local oscillator (LO), the incident wave (a_1) generated by the VSG is directly applied to the DUT, and the transmitted wave (b_2) at the output port is acquired by the VSA.

The most widely adopted metric to assess the wideband modulation distortion, through set-ups like the one in Fig. 1a, is the Error Vector Magnitude (EVM) [13]:

$$\text{EVM} = \sqrt{\frac{\sum_{n=1}^{N} |S_n^r - S_n|^2}{\sum_{n=1}^{N} |S_n|^2}}, \tag{1}$$

S_n^r being the nth received modulation symbol, S_n the corresponding symbol of the reference (ideal) constellation, and N the number of acquired symbols. The estimation of EVM is typically performed in time domain on the measured envelope waveforms. As the signal is received, part of the acquired waveform is used to recognize the modulation scheme and to reconstruct the reference signal

through the identification of a linear time-invariant (LTI) equalization filter at each signal frame, thus allowing to estimate the EVM on the remainder of the received symbols.

However, guaranteeing accurate envelope waveform measurements up to microwave frequencies across wide BWs represents a critical aspect due to the low Signal-to-Noise Ratio (SNR) of the down-conversion/receiver acquisition path. Relatively high noise levels impose a lower bound on the minimum detectable EVM and limit the overall time-domain EVM measurement accuracy. In addition, envelope measurements imply the adoption of onerous waveform measurement traceability [14, 15]. In this context, various techniques [16, 17] to estimate the EVM by frequency-domain analysis without the need for envelope demodulation have gained renewed interest, and new implementations have been recently proposed [18, 19, 20]. In these cases, custom periodic test signals are designed to match the statistical properties of the target modulation [21, 22, 20]. In [20], it is shown that wideband EVM characterization can be obtained with

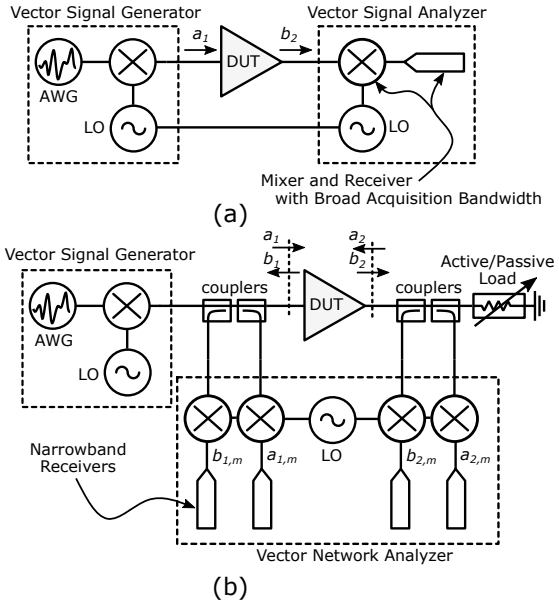

Figure 1: (a) Set-up for EVM measurement using a Vector Signal Analyzer. (b) Set-up for EVM measurement using a Vector Network Analyzer [12].

a Vector Network Analyzer (VNA) from frequency-swept narrowband relative measurements.

In effect, another substantial limitation of the set-up in Fig. 1a concerns the impossibility to identify well defined measurement reference planes up to the DUT ports, given that only one electrical variable is measured at the input and output side, respectively. Hence, the measured EVM will actually embed any residual hardware impairments of the VSG/VSA, and will not account for source/load mismatch. As a consequence, the ideality of VSG/VSA interface should be guaranteed by the manufacturer, and VSA-based set-ups are nowadays mostly used for the performance analysis of impedance-matched systems only. If the final design does not respect the EVM specifications, investigating the source of EVM impairment up to the transistor level and across the various internal PA stages becomes a complex task. Moreover, no straightforward characterization solution is yet available for applications inherently involving dynamic load modulation at the output port, e.g., variable antenna back-scattering [23] or mutual coupling in PA arrays [24].

When the DUT is terminated with a mismatched load, not only the transmitted wave (b_2), but also a non-zero wave reflected by the load (a_2) is found at the DUT output. Moreover, several additional linear networks are typically cascaded to the basic active DUT within the RF system. As these might not be properly matched across the full wide BW of operation, non-zero transmitted/reflected waves are generated at each internal interface up to the output port. In theory, each of these interfaces configures a separate non-linear dynamic system featuring a certain EVM performance. Indeed, the EVM displayed by the active DUT only is, in general, different from the one shown by the DUT cascaded with a certain linear network, or the one of the complete PA. Even at the same reference plane, calculating the EVM from either the transmitted or reflected wave could deliver different values. In general, it could be argued that the residual EVM due to the DUT only might not provide useful information with respect to the behaviour of the finalized PA.

This work addresses these aspects by providing a novel system-level analysis

of the EVM measurement process for a non-linear component cascaded with a generic linear network, a description also encompassing the case of an active DUT in the presence of wideband load mismatch. This analysis provides the basic justification for joint EVM and load-pull characterization at an internal plane of the PA (e.g., at the transistor plane), aimed at finding the particular wideband load termination for optimum EVM performance [25]. At the same time, experimental counterexamples for specific frequency-dependent loads are also provided, reporting non-negligible differences between the EVM calculated on the different waves resulting from impedance mismatch.

To develop this study, we adopt a measurement model based on the Best Linear Approximation (BLA) framework [19], which allows to perform EVM characterization in the frequency domain. This is implemented by using the VNA-based set-up in Fig. 1b, where the subscript m stands for the quantities directly measured by the VNA receivers, i.e., the waves (in practice, voltages) at the coupled arms of the couplers after frequency down-conversion. Using standard VNA techniques, calibrated reference planes can be defined at the DUT ports. Similarly to [20], the wideband EVM is obtained from narrowband relative measurements swept across the excitation frequency, allowing to quantify the residual EVM degradation due to the DUT only.

Whereas the contribution in [12] only depicted a preliminary model description and considered a reduced set of load-pull experiments just using a flat-amplitude passive tuner, here we provide a complete system-level analysis and we develop a novel wideband active load-pull (WALP) implementation enabling the accurate synthesis of user-defined load profiles across frequency at the DUT reference plane. This is achieved by generating a suitable modulated power injection using a new iterative algorithm which, just as the EVM measurement process, is likewise based on frequency-swept relative measurements only, thus avoiding envelope measurement/demodulation. These functionalities realize joint modulation distortion quantification and load-pull across BWs that could seamlessly exceed the limitations by IQ down-conversion in VSAs, possibly extending across to the full BW of the VNA test-set (i.e., for several GHz

and beyond). To the extent of this contribution, this flexibility is exploited to synthesize load profiles that are particularly irregular across frequency. For an accurate analysis, the EVM estimates for a PA across these experimental cases are here provided with associated uncertainty. While the highlighted cases display meaningful differences in EVM depending on the wave used for calculation, such irregular terminations do not normally appear in typical PA applications.

The article is organized as follows. Section 2 describes the EVM measurement model and its adaptation to the novel configuration of a mismatched DUT. Section 3 discusses the experiments performed with a VNA-based set-up using a passive tuner. The newly proposed implementation of the WALP technique in combination with the EVM analysis in the presence of frequency-dependent wideband loads is reported in Sec. 4, along with the discussion on EVM measurement accuracy. Conclusions are drawn in Sec. 5.

2. System-Level Analysis

2.1. Measurement-based EVM model

The BLA framework [19, 26, 27] allows for the identification of an optimal (in the least-square sense) linear dynamic approximation of the DUT for a given excitation class. Considering a generic input spectrum $X(f)$, the output spectrum $Y(f)$ for any non-linear dynamic period-preserving system can be represented as:

$$Y(f) = G_{YX}(f)X(f) + D_{YX}(f) + N_Y(f); \tag{2}$$

where G_{YX} is the BLA for the frequency response function (FRF) of the system across all the excitations for a certain signal class [26]; $D_{YX}(f)$ is a zero-mean value with variance $\sigma^2_{D_{YX}}(f)$ which corresponds the non-linear stochastic distortions not correlated with the input; $N_Y(f)$, with variance $\sigma^2_{N_Y}(f)$, quantifies the additive measurement noise. Using the model in (2), which corresponds to the system-level diagram in Fig. 2a, the EVM_{YX} can be obtained as [19]:

$$\mathrm{EVM}_{YX} = \sqrt{\frac{\int_{\mathrm{BW}} \sigma^2_{D_{YX}}(f)df}{\int_{\mathrm{BW}} |G_{YX}(f)|^2 S_{XX}(f)df}} \tag{3}$$

where $S_{XX}(f)$ is to the input power spectral density (PSD), and $|G_{YX}(f)|^2 S_{XX}(f)$ is the PSD linearly correlated with the input across the excited BW. The purely non-linear distortion power results:

$$\sigma^2_{D_{YX}}(f) = S_{YY}(f) - |G_{YX}(f)|^2 S_{XX}(f), \tag{4}$$

where $S_{YY}(f)$ is the output PSD. In practice, the estimation and compensation of G_{YX} in (3) corresponds to the linear receiver equalization and constellation de-rotation found in VSAs, while the EVM corresponds to the residual uncorrelated non-linear distortion contribution.

Let $X(f)$ be a periodic random-phase multi-tone input signal with flat amplitude at excitation frequencies f_l, $l = 1, \ldots, L$ across BW. When $X(f)$ is composed by a sufficiently high number of tones, its statistical properties can match any other excitation with the same PSD and complex-gaussian envelope probability density function (PDF) [19, 28, 20]. Hence, such a multi-tone excitation is formally equivalent to OFDM signals [29], allowing for a general, standard-independent methodology.

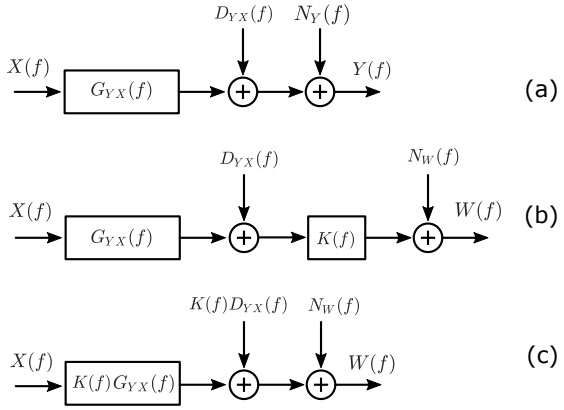

Figure 2: Measurement-based EVM model for (a) a non-linear dynamic system; (b) a non-linear dynamic system cascaded with a linear one, indicated by $K(f)$; and (c) for a non-linear dynamic system configuration corresponding to the one in (b) [12].

The FRF at each f_l is

$$G_{YX}^{[r,p]}(f_l) = \frac{Y(f_l)^{[r,p]}}{X(f_l)^{[r,p]}}; \quad \begin{matrix} r = 1, \ldots, R; \\ p = 1, \ldots, P; \end{matrix} \tag{5}$$

where P is the number of multiple acquisitions for each of the R different realizations of the input. The average of $G_{YX}^{[r,p]}$ across the P periods allows for the estimation of the noise variance $\sigma^2_{G_N}(f_l)$ of $G_{YX}(f_l)$, whereas the average across the R realizations leads to characterize the distortion power $\sigma^2_{G_D}(f_l)$ and, ultimately, $G_{YX}(f_l)$ [26]. It holds that [19]:

$$\begin{aligned} \sigma^2_{D_{YX}}(f_l) &= \sigma^2_{G_D}(f_l) S_{XX}(f_l); \\ \sigma^2_{N_{YX}}(f_l) &= \sigma^2_{G_N}(f_l) S_{XX}(f_l); \end{aligned} \tag{6}$$

so that the EVM as from (3) can be eventually obtained, while the integration in (3) becomes a sum across the L excitation frequencies.

To identify the FRF in (5), wideband waveform measurements, e.g., from a VSA, could be performed. In this work, the FRF is instead obtained from calibrated relative measurements with a VNA [20]. Indeed, the FRF can be identified by standard synchronous VNA relative measurements of the DUT complex gain, swept across the L excited frequencies. The VNA calibration corresponds to the one used for classical multi-port measurements, using procedures such as the short-open-load-thru (SOLT) calibration and its variants. The additional receiver power calibration allows to acquire power-calibrated quantities referred to the DUT reference planes. From this experimental data, the calibrated ratio between any two signals of interest can be eventually obtained in post-processing.

2.2. EVM under load mismatch

Let us consider the VNA-based set-up in Fig. 1b and a frequency domain representation for the wave variables. The EVM measurement model described in Sec. 2.1 is usually applied to matched devices, meaning that the load reflection coefficient at port 2 $\Gamma_L(f) = \frac{A_2(f)}{B_2(f)} = 0$ and, correspondingly, the incident wave at port 2 $A_2(f) = 0$. The incident wave at port 1 $A_1(f)$ corresponds to

the input signal $X(f)$ in (2), while the transmitted wave at port 2 $B_2(f)$ to the output signal $Y(f)$, resulting in the calculation of $\mathrm{EVM}_{B_2A_1}$ as from (3).

Under load mismatch conditions ($\Gamma_L(f) \neq 0$), the large-signal operating point (LSOP) of the DUT will be modified, thus implying, in general, a different distortion performance and a correspondingly different EVM value. Still, regardless of the actual distortion involved, it is worth analyzing the EVM measurement process in the sense that both $B_2 \neq 0$ and $A_2 \neq 0$, meaning that two non-null wave-variables are present at the DUT output port. In particular, the analysis should clarify if $\mathrm{EVM}_{B_2A_1}$ is still an effective metric in representing the modulation distortion of the DUT. Indeed, it could be argued that the distortion measured by using the reflected wave $A_2(f) = \Gamma_L(f)B_2(f)$ as the output wave-variable in (2) is, in general, different from the one measured by using $B_2(f)$. This could result in a calculation of the $\mathrm{EVM}_{A_2A_1}$ value different from $\mathrm{EVM}_{B_2A_1}$, despite the LTI relationship between $B_2(f)$ and $A_2(f)$ imposed by the load termination $\Gamma_L(f)$ which, in turn, implies $\mathrm{EVM}_{A_2B_2} = 0$ by definition. In any case, the existence of possibly different EVM values should raise the doubt on which is the *correct* one to assess the DUT performance and, more in general, on how the EVM quantity is propagated by LTI systems.

Then, let us adapt the system-level measurement model of Fig. 2a to the case of a non-linear dynamic system cascaded with a LTI network (Fig. 2b) defined by its FRF $K(f)$. The signal at the output of the two cascaded blocks is $W(f) = K(f)\tilde{Y}(f)$, where $\tilde{Y}(f)$ is $Y(f)$ without additive noise (which is independent from all the other quantities):

$$\tilde{Y}(f) = Y(f) - N_Y(f) = G_{YX}(f)X(f) + D_{YX}(f). \tag{7}$$

Then, the EVM model in (2) applied to $W(f)$, including the corresponding additive noise contribution $N_W(f)$, results:

$$\begin{aligned} W(f) &= G_{WX}X(f) + D_{WX}(f) + N_W(f) = K(f)\tilde{Y}(f) + N_W(f) \\ &= K(f)G_{YX}(f)X(f) + K(f)D_{YX}(f) + N_W(f). \end{aligned} \tag{8}$$

Hence, the following relationships hold:

$$G_{WX}(f) = K(f)G_{YX}(f); \quad D_{WX}(f) = K(f)D_{YX}(f); \tag{9}$$

which imply that the cascaded linear FRF multiplies both the BLA and the nonlinear stochastic distortion associated to the original system. The expression in (8) is represented in the block diagram of Fig. 2c, and it is equivalent to the one in Fig. 2b. From (8) it holds:

$$\mathrm{EVM}_{WX} = \sqrt{\frac{\int_{\mathrm{BW}} \sigma^2_{D_{WX}}(f)df}{\int_{\mathrm{BW}} |G_{WX}(f)|^2 S_{XX}(f)df}} = \sqrt{\frac{\int_{\mathrm{BW}} |K(f)|^2 \sigma^2_{D_{YX}}(f)df}{\int_{\mathrm{BW}} |K(f)|^2 |G_{YX}(f)|^2 S_{XX}(f)df}}. \tag{10}$$

The comparison between the expression in (10) and the one in (3) entails that, in general, $\mathrm{EVM}_{WX} \neq \mathrm{EVM}_{YX}$. At the same time, if the amplitude response of the cascaded LTI network is flat across frequency, i.e., $|K(f)| = K \ \forall f \in \mathrm{BW}$, the quantities $|K(f)|^2$ at both numerator and denominator can be moved out from the integrals in (10), so that eventually $EVM_{WX} \equiv EVM_{YX}$. More in general, by considering the upper and lower bound of $|K(f)|^2$ within the BW, it can be shown that:

$$\sqrt{\frac{\min\limits_{f\in\mathrm{BW}} |K(f)|^2}{\max\limits_{f\in\mathrm{BW}} |K(f)|^2}}\mathrm{EVM}_{YX} \leq \mathrm{EVM}_{WX} \leq \sqrt{\frac{\max\limits_{f\in\mathrm{BW}} |K(f)|^2}{\min\limits_{f\in\mathrm{BW}} |K(f)|^2}}\mathrm{EVM}_{YX}. \tag{11}$$

By applying this system-level description and the corresponding wave-variable notation to the actual DUT under load mismatch, in general it holds that $\mathrm{EVM}_{B_2A_1} \neq \mathrm{EVM}_{A_2A_1}$, whereas $\mathrm{EVM}_{B_2A_1} \equiv \mathrm{EVM}_{A_2A_1}$ if the modulus of $\Gamma_L(f)$ (corresponding to the one of $K(f)$ in the system-level description of Fig. 2) is flat across the BW. This result implies practical consequences in the modulation distortion quantification of DUTs at different loading conditions, and it is of interest to analyze whether the conditions in (11) are encountered in realistic load-pull scenarios.

3. Passive Load-Pull Measurements

3.1. Measurement Set-up

A first implementation of the set-up used for the experiments, based on a Keysight PNA-X N5242A VNA, is reported in Fig. 3. To enable load-pull, the load of the DUT is imposed by a cascaded manual slide screw tuner (Maury Microwave 7941A). The tuner embodies a tunable two-port linear network modelled by the scattering transfer matrix $\mathbf{T}_{32}(f)$, imposing

$$\begin{bmatrix} A_3(f) \\ B_3(f) \end{bmatrix} = \mathbf{T}_{32}(f) \begin{bmatrix} A_2(f) \\ B_2(f) \end{bmatrix}; \quad \text{with } \mathbf{T}_{32}(f) = \begin{bmatrix} t_{32}^{11}(f)\ t_{32}^{12}(f) \\ t_{32}^{21}(f)\ t_{32}^{22}(f) \end{bmatrix}. \tag{12}$$

While providing an adjustable load for experimentally testing if $\mathrm{EVM}_{B_2A_1} = \mathrm{EVM}_{A_2A_1}$ in different loading conditions, the set-up in Fig. 3 allows to replicate

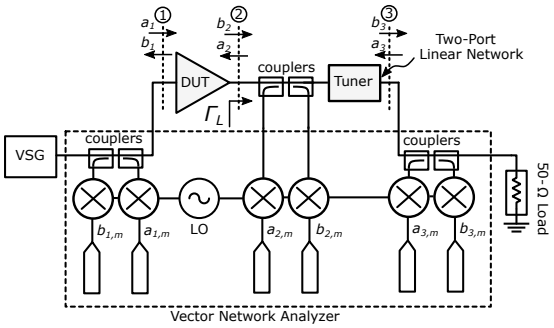

(a)

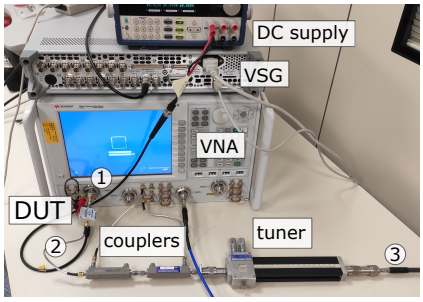

(b)

Figure 3: Block diagram (a) and photo (b) of the measurement set-up implemented for EVM characterization using a Vector Network Analyzer, including a passive tuner at the load of the DUT [12].

the common case of a PA cascaded by a two-port matching network, which is in turn terminated on a 50-Ω load. Therefore, it is possible to check if the equivalence of the measured EVM values is also observed on the transmitted $B_3(f)$, which is the signal usually considered for classical distortion measurements using 50-Ω-matched equipment like VSAs ($A_3(f) = 0$ in this case). In fact, the $A_2(f)$ and $B_2(f)$ waves are standing at the reference plane before the output matching network, which is normally inaccessible when testing the finalized PA.

Then, three ports (thus, three calibration reference planes) have been identified in Fig. 3, where each port makes use of two directional couplers for wave sensing (in particular, internal couplers of the VNA for ports 1 and 3, external couplers for port 2). Port 1 and 2 are at the input and the output of the PA, respectively, while Port 3 is the one after the tuner. A three-port SOLT relative calibration and a receiver power calibration (traced to power meter measurements) was implemented. The modulated input signal at RF is generated by a Keysight MXG N5182B VSG, which is connected to the rear-panel of the VNA and re-directed internally to inject into port 1. The DUT is an off-the-shelf PA from Mini-Circuits (ZFL-11-AD+) operating from 2 MHz to 2 GHz.

3.2. Experimental results

By referring to the system-level representation of Fig. 2b and the notation introduced in Sec. 2, the following EVM configurations are considered for measurement using the three-port set-up equipped with the tuner **T** at the DUT load port (Fig. 3):

a. $\mathrm{EVM}_{B_2A_1}$, in which the output $Y(f)$ corresponds to $B_2(f)$;
b. $\mathrm{EVM}_{A_2A_1}$, in which the output $W(f)$ corresponds to $A_2(f)$ and $K(f) = -\frac{t_{32}^{12}(f)}{t_{32}^{11}(f)} = \Gamma_L(f)$;
c. $\mathrm{EVM}_{B_3A_1}$ in which the output $W(f)$ corresponds to $B_3(f)$ and $K(f) = t_{32}^{21}(f)\Gamma_L(f) + t_{32}^{22}(f)$.

All configurations use $A_1(f)$ as the input signal but different waves as output signals. The employed excitation is a 100-MHz-BW, L-tone random phase multitone signal (L =1001) with a 100-kHz frequency spacing among the tones and

centered at 1.75 GHz. The PDF of such input signal is gaussian with band-limited white PSD, reproducing a suitable test scenario as from OFDM-based 5G Frequency Range 1 standard [30]. Then, the EVM characterization routine was applied with $P = 2$ and $R = 25$ as from (5). The load tuner has been configured in two different settings, which resulted in two different $\mathbf{T}'_{32}(f)$ and $\mathbf{T}''_{32}(f)$ values and corresponding load profiles $\Gamma'_L(f)$ and $\Gamma''_L(f)$. In both cases, the wideband response of the tuner with respect to the excitation BW results in frequency profiles for $K(f)$ that are almost flat in amplitude and show a frequency-dependent phase response, as inherently determined by the tuner (see the in the inset of Fig. 4).

The experiments have been repeated at different RF available source power levels $P_{av,s}$ showing that, as could be expected, Γ_L influences the LSOP of the DUT (yet only slightly, in this specific case), thus resulting in different EVM values [12]. Nevertheless, the three configurations result to the same EVM value (up to measurement noise) for a given Γ_L confirming, as from Sec. 2.2, that the choice of the signals to be measured does not influence the EVM extraction for a flat-amplitude load termination. In such a case, any of the $B_2(f), A_2(f)$, or $B_3(f)$ can be possibly considered, while it is appropriate to select the one with the highest SNR. At the same time, it is worth recalling from [12] that the BLAs feature different values depending on the choice for the output signal. Indeed, the BLA embeds the frequency response of the cascaded linear network in each different case. Hence, the measurement model of Fig. 2b is equivalent to the general one of a non-linear dynamic system (Fig. 2a) where the BLA and the stochastic distortion contribution are multiplied by $K(f)$, leading to the configuration in Fig. 2c.

4. Active Load-Pull Measurements

4.1. VNA-based Wideband Active Load-pull

A passive tuner like the one employed in the set-up of Fig. 3 is normally used to set a load impedance at one single frequency. In fact, the whole impedance

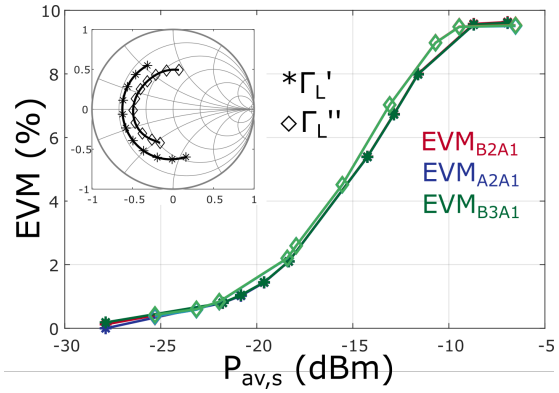

Figure 4: EVM shown as a function of RF available input power ($P_{av,s}$) for $B_2(f)$, $A_2(f)$ and $B_3(f)$, in the presence of flat-amplitude loads $\Gamma'_L(f)$ and $\Gamma''_L(f)$ (see inset) synthesized by the passive tuner [12].

profile cannot be arbitrarily imposed across a wideband frequency range, as the slide-screw tuner allows for limited mechanical degrees of freedom in adjusting the frequency response of its hardware. With hundred-MHz BWs, this typically results in a fairly flat amplitude response across the excitation BW and a linear phase rotation, whose excursion depends on the electrical delay determined by the tuner itself. The amplitude might actually display irregularities for wider BW due to the attenuation introduced by parasitic losses in the line.

To extend the capabilities of the set-up and test the implications of the EVM measurement procedure under wideband load mismatches, an additional VNA-based active load-pull functionality [31, 32] has been developed, resulting in the set-up implementation of Fig. 5. This bench includes an additional VSG used to inject power at the DUT output port, while the VNA-based acquisition section remains the same as in Fig. 3, including a two-port calibration procedure. Indeed, the tuner and the corresponding third port are not necessary in this case, as the measurements and the required active load synthesis take place directly at the DUT output port.

Given a fixed DUT excitation at the input port, a suitable signal injection at the output port allows to realize a user-defined arbitrary load profile across

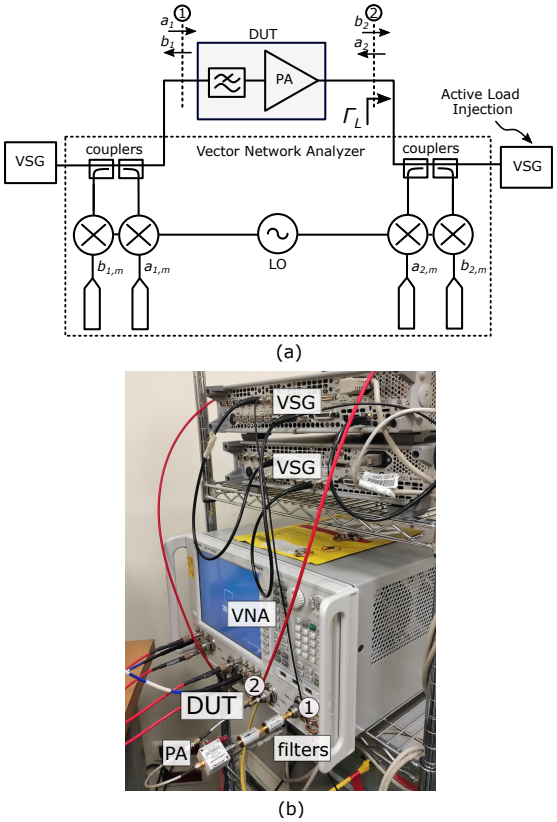

Figure 5: Block diagram (a) and photo (b) of the VNA-based measurement set-up used for EVM characterization exploiting wideband active load-pull capabilities.

the excitation BW. Let us represent the waveform injected at the output by the complex vector $\mathbf{x} = \{x_i\}$ containing the frequency components of the digital numerical signal at the N target frequencies f_i, $i = 1 \dots N$ throughout the BW of interest. A given $\mathbf{x}$ will synthesize a specific reflection coefficient profile $\mathbf{\Gamma_L} = \{\Gamma_{L,i}\}$ at the DUT output reference plane, through a specific functional mapping $\mathbf{\Gamma_L} = \mathcal{F}(\mathbf{x})$. The closed-form for such mapping is not a-priori known for a non-linear DUT [33], and generally strongly depends on the LSOP. Nevertheless, this black-box function $\mathcal{F}$ can be empirically evaluated by measuring the load reflection coefficients $\Gamma_{L,i} = \frac{A_2(f_i)}{B_2(f_i)}$ using classical VNA acquisitions at each frequency.

Then, the goal of WALP is to find the specific value $\mathbf{x_T}$ for which $\mathbf{\Gamma_L}$ equals a user-prescribed profile $\mathbf{\Gamma_T}$. This amounts to imposing that the deviation from target across all the N frequencies $\mathbf{E} = \mathbf{\Gamma_L} - \mathbf{\Gamma_T}$ equals zero. This error minimization procedure can be performed using an iterative learning control (ILC) algorithm [34], which computes the required solution through a series of successive approximations $\mathbf{x}_k$. At the k-th iteration, the next tentative solution is computed as:

$$\mathbf{x}_{k+1} = \mathbf{x}_k + \mathbf{L}_k \mathbf{E}_k, \tag{13}$$

in which $\mathbf{E}_k$ is the deviation between the measured and the target load at the given iteration, and $\mathbf{L}_k$ is a user-chosen $N \times N$ matrix called the *learning gain*. Under specific conditions on $\mathbf{L}_k$ [34], the method is guaranteed to converge to the operating regime in which $\mathbf{E}$ is exactly equal to zero, and the correct $\mathbf{\Gamma_T}$ is synthesized.

The choice of $\mathbf{L}_k$ is of paramount importance for the performance in terms of convergence speed, number of measurements, and stability of the WALP method. One optimal choice, equivalent to the use of standard Newton's method for finding zeros of unknown functions, could be that of taking $\mathbf{L}_k$ equal to the inverse of the Jacobian matrix of the function $\mathcal{F}$ at $\mathbf{x}_k$. However, given that $\mathcal{F}$ does not have a closed-form expression but it is exclusively known from measurements, the estimation of its N^2 terms would require N VNA sweeps across the whole BW. Thus, this approach is highly inefficient in terms of measurement time owing to the very large number of tones required to approximate typical communication standards.

Nevertheless, it was shown in [33] that, even in the non-linear operating region for the DUT, the overall coupling between the injected tones at a given frequency and the device response at another one is negligible with respect to the same-frequency behavior. This implies that different frequencies are only weakly coupled, and the problem can be efficiently treated as a series of N parallel optimizations. In the ILC algorithm, this amounts to the fact that the full $N \times N$ learning matrix $\mathbf{L}_k$ in (13) can be substituted by a diagonal matrix

$\mathbf{\Lambda}_k$

$$\mathbf{x}_{k+1} = \mathbf{x}_k + \mathbf{\Lambda}_k \mathbf{E}_k, \tag{14}$$

where the diagonal elements $\lambda_{k,ii}$ can be obtained from just a single VNA measurement sweep, granting a feasible measurement time at each iteration. A typical choice is to make use of the classical secants' method, for which the diagonal terms are computed as

$$\lambda_{k,ii} = -\frac{x_{k,i} - x_{k-1,i}}{E_{k,i} - E_{k-1,i}}. \tag{15}$$

While this choice has been shown to be generally suitable for performing WALP [32], the convergence and stability performance was found to be sub-optimal in case of low SNR in the measurement of $\mathbf{\Gamma_L}$. This is indeed a case of interest, as applications might require WALP for signals with low power-per-tone, such as in case of unequal excitation amplitudes, or when considering out-of-band IM and in-band notches [25]. This poor performance can be pin-pointed to the computation of the term in (15), which estimates the slope of the secant to function $\mathcal{F}$ at the last two iterations $k-1$ and k. As the method converges to the target, the values of the denominator $E_{k,i} - E_{k-1,i} = \Gamma_{L_{k,i}} - \Gamma_{L_{k-1,i}}$ becomes progressively closer to zero and largely dominated by measurement noise, which is proportionally higher in case of low power-per-tone.

Even though $\mathcal{F}$ is unknown, the load synthesized when no injection is present $\mathbf{\Gamma_0} = \mathcal{F}(\mathbf{0})$ is equal to the linear match of the output source. This term can be measured by the VNA as the standard reflection coefficient [33] that is observed when the output source is turned off. Therefore, instead of using (15), a more robust estimate can be obtained by finding the slope of the line between the reference point set by $\mathbf{\Gamma_0}$ and the last measurement:

$$\lambda_{k,ii} = -\frac{x_{k,i}}{\Gamma_{L_{k,i}} - \Gamma_{L_{0,i}}}. \tag{16}$$

This improved method, used in the following, significantly improves the stability of the WALP algorithm, while still maintaining excellent convergence speed.

4.2. Experimental Results

The described WALP technique allows to actively synthesize any arbitrary load profile, hence to generate arbitrary non-flat $\Gamma_L(f)$ across the BW. While it is indeed possible to synthesize a target load termination also across the spectral regrowth bands [25] of the $B_2(f)$ wave, here we take into account $\Gamma_L(f)$ only within the excited BW. Therefore, throughout the characterization, the out-of-band termination is left to the one natively presented by the set-up. With respect to Sec. 3, a new DUT, composed by the cascade of two connectorized low-pass filters (Mini-Circuits SLP-300+, with combined 6-dB cut-off frequency of 300 MHz) at the input, and the Mini-Circuits amplifier ZFL-11-AD+, was used for testing EVM under WALP (see Fig. 5). The chosen center frequency is fixed at f_0=325 MHz, using an excitation BW=50 MHz with a 10.5 kHz tone spacing. This excitation allows to cover a large relative BW for this DUT, resulting in a shaped frequency response and relevant testing conditions for EVM measurement. Three different actively generated load profiles are considered:

a. a fixed load flat across frequency:

$$\Gamma_L^{(a)}(f) = 0.7e^{\pi/8}, \forall f \in \mathrm{BW}; \tag{17}$$

b. a stepped-amplitude load profile across the two half-bands:

$$\Gamma_L^{(b)}(f) = \begin{cases} 0.7e^{\pi/8} & f_0 - \frac{\mathrm{BW}}{2} < f < f_0 \\ 0 & \text{otherwise} \end{cases}; \tag{18}$$

c. a complementary stepped-amplitude profile to $\Gamma_L^{(b)}(f)$:

$$\Gamma_L^{(c)}(f) = \begin{cases} 0.7e^{\pi/8} & f_0 < f < f_0 + \frac{\mathrm{BW}}{2} \\ 0 & \text{otherwise} \end{cases}. \tag{19}$$

The use of these extreme stepped-amplitude cases, which are hardly realizable using passive physical components, allows to fully explore the implications of a broadband load mismatch on the EVM measurement procedure. These configurations are reported in Fig. 6 using the system-level representation, along with the notation already used in Sec. 2.2.

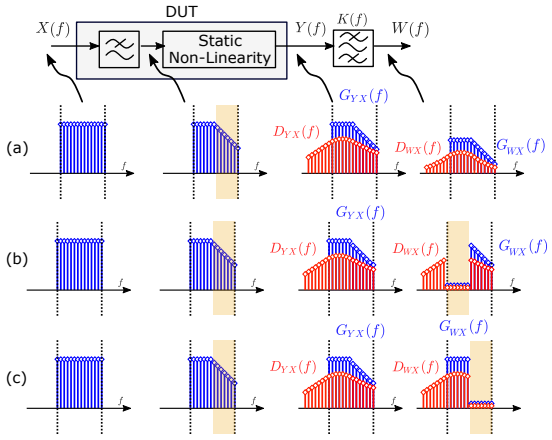

Figure 6: Block diagram representation describing the experiment for the calculation of EVM_{YX} and EVM_{WX} in the presence of active load injection emulating a cascaded linear network $K(f)$. The considered DUT includes a low-pass filter as from Fig. 5.

In order to compare EVM values in different cases, the DUT was excited using $P = 2$ periods of $R = 120$ realizations of a flat-amplitude random-phase multi-tone signal with power $P_{av,s} = -5.5$ dBm covering the 50 MHz BW of interest around f_0. In particular, the use of a flat and sufficiently high amplitude for the excitation tones allows to maximize the repeatability of $\Gamma_L(f)$ (see Sec. 4.3). The BLA decomposition into LTI, distortion, and noise components, as from the procedure in Sec. 2.1, was performed on the $A_2(f)$ and $B_2(f)$ waves for each of the three different load profiles, hence providing all quantities to calculate the EVM in each of the conditions. The frequency domain plot of the different contributions are shown in Fig. 7. When measuring $\mathrm{EVM}_{A_2A_1}$, coherently with the target $\Gamma_L^{(b)}(f)$ and $\Gamma_L^{(c)}(f)$ in (18) and (19), respectively, the linearly correlated $A_2(f) = \Gamma_L(f)B_2(f)$ is zero (up to the measurement noise) for part of the passband (see Figs. 7(d) and 7(f)). The noise shaping on the σ_N^2 contribution is due to Intermediate-Frequency (IF) calibration, as the power spectra measured with the VNA receivers are reconstructed by sequentially acquiring 30-MHz-wide segments exploting the method in [35] (the same noise shaping can also be seen in Fig. 8 on the PSD of $A_1(f)$).

Both the BLA estimation and the resulting EVM are affected by measure-

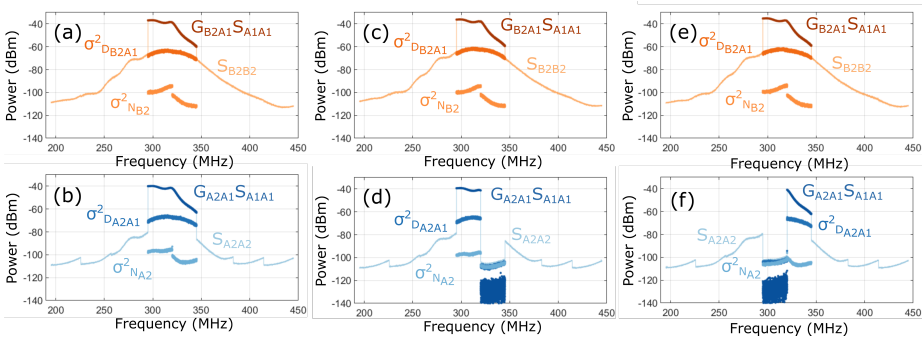

Figure 7: PSDs of the various components in the BLA analysis of the filter-PA cascade DUT for the actively synthesized loads. (a), (c), (e) (top row) refer to the quantities for $\mathrm{EVM}_{B_2A_1}$; (b), (d), (f) (bottom row) to the ones for $\mathrm{EVM}_{A_2A_1}$. The reflection coefficients are $\Gamma_L^{(a)}(f)$ in (a) and (b) (first column); $\Gamma_L^{(b)}(f)$ in (c) and (d) (second column); $\Gamma_L^{(c)}(f)$ in (e) and (f) (third column). The input spectrum is equal in all cases to the one reported in Fig. 8.

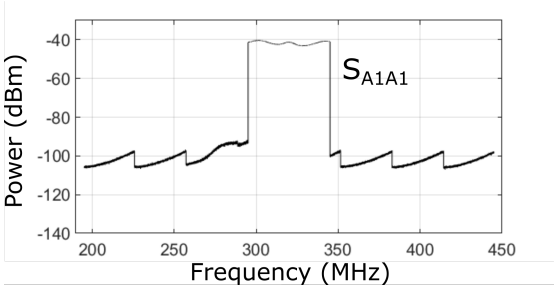

Figure 8: Measured input PSD of a 50-MHz wide random phase multi-tone signal around f_0=325 MHz with available source power of $P_{av,s} = -5.5$ dBm.

ment noise and by the imperfect approximation of the statistical expectation values from the finite realizations number $R = 120$ of the underlying stochastic process. These aspects become critical when considering possibly small differences between the measured values of $\mathrm{EVM}_{A_2A_1}$ and $\mathrm{EVM}_{B_2A_1}$. In fact, one should rather assess if any difference between the two values is statistically meaningful with respect to their associated uncertainty.

In principle, all the $R = 120$ realizations should be used in order to get the most precise estimate of the EVM value, as done in Sec. 3.2. With this approach, however, no uncertainty quantification can be extracted from the

same dataset. In order to provide estimates of $\mathrm{EVM}_{A_2A_1}$ and $\mathrm{EVM}_{B_2A_1}$ with associated uncertainties, the given $R = 120$ signal realizations are split into $S = 60$ subgroups with two realizations each. This is the minimum number of realization allowing to separate noise and non-linear stochastic distortions via the robust BLA method [28]. The BLA analysis is then performed on each subgroup, obtaining a total of $S = 60$ different EVM estimates. Then, coherently with the GUM [36], the result of the EVM measurement is taken as the sample mean across the S subgroups, and the associated uncertainty is the sample standard deviation divided by the number S of subgroups (type-A uncertainty). While the use of more realizations for estimating each EVM would lead to a lower standard deviation among the different groups (as noise would be averaged out and the expectations would be closer to their asymptotic values), less information would be available for evaluating the uncertainty for a fixed total number of measurements.

The histograms of $\mathrm{EVM}_{A_2A_1}$ and $\mathrm{EVM}_{B_2A_1}$ for the three load profiles under test are shown in Fig. 9. The resulting sample means and associated uncertainties are instead reported in Table 1. As expected from the system-level analysis and observed with passive load-pull, the flat $\Gamma_L^{(a)}(f)$ case shows that the difference between the two EVM values is less than the estimated uncertainty. Instead, the $\Gamma_L^{(b)}(f)$ and $\Gamma_L^{(c)}(f)$ stepped profiles show a difference between the means that is several times the associated uncertainty, definitely meaning that two different EVM values can be observed depending on the considered wave. While it is unknown whether the measured EVM values display a gaussian distribution, the sample means computed on a sufficiently large number of independent experiments S are expected to converge to a gaussian distribution. Therefore, the results reported in Table 1 can also be used to provide confidence intervals [36].

To further validate the framework, the mean $\mathrm{EVM}_{A_2A_1}$ value can be compared with the prediction as from Sec. 2.2. In this case, the prediction is obtained by using the measured values for $\sigma^2_{D_{B_2A_1}}(f)$ and $\Gamma_L(f)$ on the whole dataset of $R = 120$ realizations, using (10) in order to find a predicted $\mathrm{EVM}_{A_2A_1}$.

Load	$\mathrm{EVM}_{A_2A_1}(\%)$	$u(\mathrm{EVM}_{A_2A_1})(\%)$	$\mathrm{EVM}_{B_2A_1}(\%)$	$u(\mathrm{EVM}_{B_2A_1})(\%)$	Predicted $\mathrm{EVM}_{A_2A_1}(\%)$
$\Gamma_L^{(a)}(f)$	5.695	0.012	5.694	0.012	5.694
$\Gamma_L^{(b)}(f)$	10.339	0.019	5.515	0.012	10.356
$\Gamma_L^{(c)}(f)$	5.306	0.015	6.395	0.013	5.303

Table 1: Estimate and standard uncertainty computed from $S = 60$ measured EVM values, using two realizations in each, for the actively synthesized loads under exam. For the $A_2(f)$ case, a comparison with the theoretically predicted value is also reported.

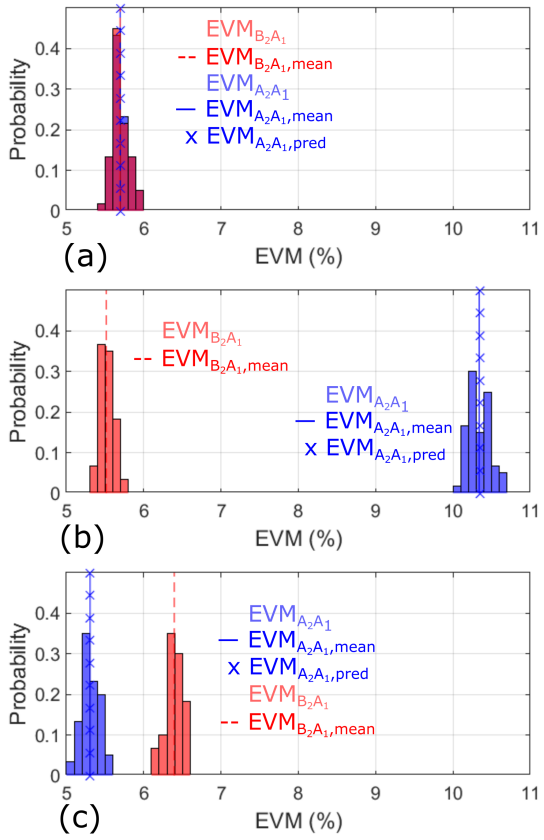

Figure 9: Histogram of $S = 60$ measured EVM values, using 2 realizations in each, for the actively synthesized loads (a) $\Gamma_L^{(a)}(f)$, (b) $\Gamma_L^{(b)}(f)$, (c) $\Gamma_L^{(c)}(f)$. The sample means and the theoretically predicted $\mathrm{EVM}_{A_2A_1}$ are also reported.

The experimental results are in close agreement with the theoretically predicted value for all the examined loads (see Table 1).

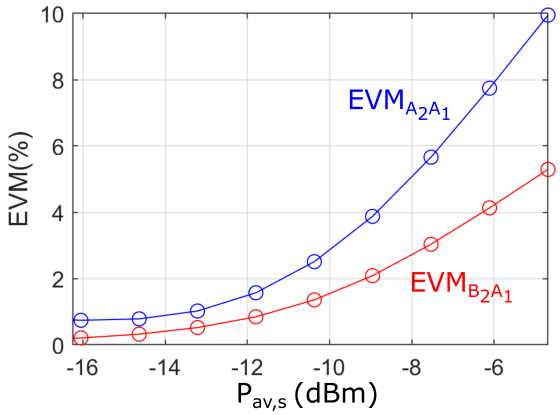

Figure 10: EVM profile as a function of $P_{av,s}$ for $B_2(f)$, $A_2(f)$, for the stepped-amplitude load $\Gamma_L^{(b)}(f)$.

A power sweep was performed in order to monitor the evolution of the distortion performance on the $A_2(f)$ and $B_2(f)$ waves for the $\Gamma_L^{(b)}(f)$ profile, which presents the most significant deviation in the previous tests. In this new test, each EVM is computed by jointly using $P = 2$ periods of $R = 15$ realizations per power value, with the results being shown in Fig. 10. The $\text{EVM}_{A_2A_1}$ and $\text{EVM}_{B_2A_1}$ start from similar values and progressively diverge for higher powers. Indeed, for low power levels both waves should display negligible distortion (i.e., EVM=0), as the DUT operates linearly (the slightly different residual EVM levels at low power are due to different SNR levels on the measurements of the $A_2(f)$ and $B_2(f)$ waves).

4.3. Load repeatability using WALP

Whereas the reflection coefficient of a passive load is strictly LTI, it could be argued that the active load synthesis by WALP is subject to slight differences at each signal realization. Indeed, the iterative WALP procedure of Sec. 4.1 must be re-run at each signal realization given that a different output injection is required to set the same load profile for each of the many different input realization requested in the EVM measurement procedure. This could, in principle, cause different LSOPs and, correspondingly, different EVM values, also in case

of a flat target impedance yet not perfectly synthesized by WALP.

Therefore, WALP has to be evaluated in terms of its capability of setting a correct and repeatable load in each case. Similarly to (5), a BLA analysis is performed on the measured load at each run, on the same dataset previously used with $R = 120$, $P = 2$:

$$\Gamma_L^{[r,p]}(f_l) = \frac{A_2(f_l)^{[r,p]}}{B_2(f_l)^{[r,p]}}; \quad \begin{matrix} r = 1, \ldots, R; \\ p = 1, \ldots, P. \end{matrix} \tag{20}$$

Hence, the overall BLA for Γ_L, the variance of the noise of the reflection coefficient measurements σ^2_{N,Γ_L}, and the variance of the non-linear stochastic distortions σ^2_{D,Γ_L} can be computed [28]. The results for the three load profiles of Sec. 4.2 are reported in Fig. 11.

From the same dataset, one can also extract the noise variance on the BLA $\sigma^2_{\Gamma_L,n}$ [28], which indicates a minimum detection level for the distortion involved. This quantity results to be below the noise level of a single measurement (σ^2_{N,Γ_L}) due to the averaging effect obtained by jointly considering $R \times P$ measurements. The frequency shaping of $\sigma^2_{\Gamma_L,n}$, proportionally increasing with frequency, can be attributed to the decaying frequency response of the $B_2(f)$ wave due to the effect of the input low-pass filters within the DUT. Since the load reflection coefficient is estimated as a ratio between the $A_2(f)$ and $B_2(f)$ waves, the SNR is proportionally lower for those frequencies at which the DUT generates less output power [33].

For an ideal LTI load like one synthesized by a passive tuner, the total noise variance $\sigma^2_{\Gamma_L,n}$ corresponds to the σ^2_{D,Γ_L} component at each frequency as, by definition, an LTI load does not involve any incremental distortion with respect to the detection level. Instead, for all the three profiles under test, the measured loads synthesized by WALP display σ^2_{D,Γ_L} greater than $\sigma^2_{\Gamma_L,n}$, hinting to an imperfect repeatability across the realizations and a sub-optimal emulation of the LTI case. Nevertheless, this behavior can be explained by the fact that the WALP algorithm uses actual measurements in order to converge to the required target load. Hence, the final accuracy on the load synthesized at the end of

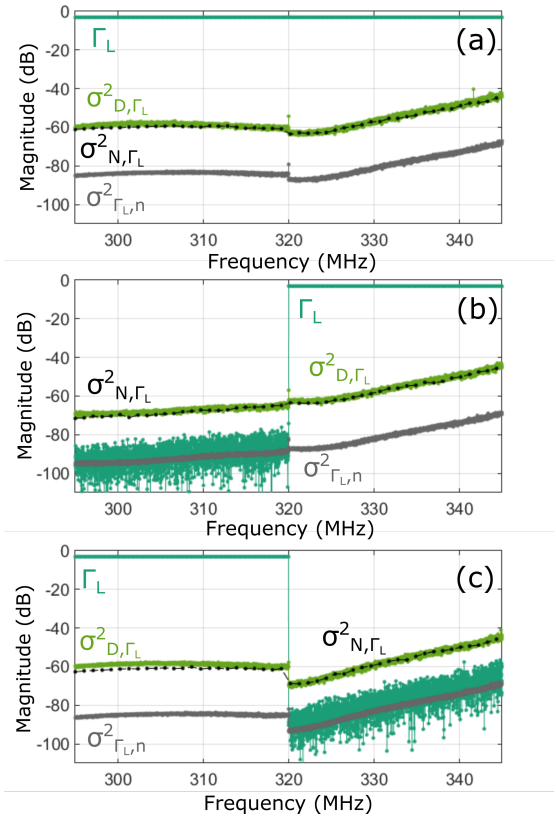

Figure 11: Load reflection coefficient Γ_L (BLA estimate), variance of the noise of the reflection coefficient measurements σ^2_{N,Γ_L}, variance of the non-linear stochastic distortions σ^2_{D,Γ_L}, and noise variance on the BLA $\sigma^2_{\Gamma_L,n}$ for the actively synthesized loads (a) $\Gamma_L^{(a)}(f)$, (b) $\Gamma_L^{(b)}(f)$, (c) $\Gamma_L^{(c)}(f)$.

the iterative procedure is clearly limited by the measurement noise σ^2_{N,Γ_L}. In effect, the fact that the load distortion σ^2_{D,Γ_L} closely matches the noise σ^2_{N,Γ_L} on each acquisition demonstrates that the proposed WALP algorithm can reach this lower theoretical limit, and that this WALP implementation is suitable for the proposed EVM analysis. Overall, for the conditions under examination, the repeatability of the load is of the order of -60 dB to -40 dB depending on the frequency. This can be taken as a satisfactory level, as the LSOP of the DUT is not expected to have significant variations for such small differences.

5. Conclusion

This article investigated VNA-based measurement procedures for evaluating the wideband modulation distortion of RF PAs in the presence of load mismatch conditions. The described functionalities allow to measure EVM at particular reference planes within the RF system across arbitrarily wide measurement BWs, avoiding the typical constraints due to the limited BW of the receiver. In addition, the experiments exploited different techniques to impose arbitrary load terminations, either by means of a classical passive tuner, or through a novel wideband active load-pull method. In particular, the latter allows for extreme flexibility in synthesizing frequency-dependent load profiles, enabling the configuration of meaningful test cases for considering the implications of load-pull on the EVM measurement.

System-level analysis and experimental evidence have shown that, in general, the measured EVM value depends on the wave variables chosen for EVM calculation, either this being the transmitted or reflected wave at the DUT output port, or the wave at the interface of a cascaded LTI network. At the same time, the EVM is analytically found to be the same for a flat-amplitude LTI network cascaded to the DUT, regardless of the wave chosen for EVM calculation. Such a case should be applicable to electron devices or sub-systems displaying sufficient wideband behaviour, as they likely feature optimal load terminations that are flat across the target BW. Electrical delays, such as those introduced by transmission lines, imply only a phase rotation of the load, without compromising amplitude flatness. While irregular impedance profiles could be fabricated on purpose (as done here), the use of such non-standard terminations is quite rare in PA applications and pertains to anomalous active device behavior. Even in this case, the EVM differences across the wave variables might still be relatively low, depending on the actual frequency response of the cascaded LTI system.

Overall, the study demonstrates that, in realistic PA applications, the EVM can be independently extracted from any wave quantity at the load port or at the interface of a cascaded liner network, allowing to choose the one measured

with the maximum SNR. In effect, provided that the excitation falls under a well-defined signal class, this study clarifies that the EVM obtained using the implemented measurement procedure quantifies the modulation distortion induced by the active device, and it can actually be seen as a network metric specific to the DUT rather than a metric extracted from the output signal, as usually intended for VSA-based techniques. As a consequence, the EVM can be employed as a figure-of-merit in the presence of unmatched components throughout the design phase, enabling load-pull experiments for finding the optimum termination, and effectively resulting in an improved measurement-based design cycle for wideband high-linearity PAs.

References

[1] K. A. Remley, et al., Measurement challenges for 5g and beyond: An update from the national institute of standards and technology, IEEE Microw. Mag. 18 (5) (2017) 41–56.

[2] C. Arnaud, D. Basataud, J. Nebus, J. Teyssier, J. Villotte, D. Floriot, An active pulsed rf and pulsed dc load-pull system for the characterization of hbt power amplifiers used in coherent radar and communication systems, IEEE Trans. Microw. Theory Techn. 48 (12) (2000) 2625–2629.

[3] G. P. Gibiino, A. Santarelli, P. A. Traverso, Pulsed techniques for the characterization of low-frequency dispersive effects in rf power fets using a flexible measurement set-up, Measurement 176 (2021) 109240.

[4] N. B. De Carvalho, J. C. Pedro, Large-and small-signal imd behavior of microwave power amplifiers, IEEE Trans. Microw. Theory Techn. 47 (12) (1999) 2364–2374.

[5] G. P. Gibiino, A. M. Angelotti, A. Santarelli, C. Florian, Microwave characterization of trapping effects in 100-nm gan-on-si hemt technology, IEEE Microw. Wirel. Compon. Lett. 29 (9) (2019) 604–606.

[6] J. H. Vuolevi, T. Rahkonen, J. P. Manninen, Measurement technique for characterizing memory effects in rf power amplifiers, IEEE Trans. Microw. Theory Techn. 49 (8) (2001) 1383–1389.

[7] M. Alizadeh, D. Rönnow, A two-tone test for characterizing nonlinear dynamic effects of radio frequency amplifiers in different amplitude regions, Measurement 89 (2016) 273–279.

[8] V. Gillet, M. Bouslama, J.-P. Teyssier, M. Prigent, J.-C. Nallatamby, R. Quéré, An unequally spaced multi-tone load–pull characterization technique for simultaneous linearity and efficiency assessment of rf power devices, IEEE Trans. Microw. Theory Techn. 67 (7) (2019) 2505–2513.

[9] G. P. Gibiino, A. M. Angelotti, A. Santarelli, F. Filicori, P. A. Traverso, Multitone multiharmonic scattering parameters for the characterization of nonlinear networks, IEEE Trans. Instrum. Meas. 70 (2020) 1–12.

[10] A. M. Angelotti, G. P. Gibiino, C. Florian, A. Santarelli, Broadband error vector magnitude characterization of a gan power amplifier using a vector network analyzer, in: IEEE MTT-S Int. Microw. Symp., IEEE, 2020, pp. 747–750.

[11] K. Fu, C. L. Law, T. T. Thein, Test bed for power amplifier behavioral characterization and modeling, Measurement 46 (8) (2013) 2735–2745.

[12] See attached conference article. Details omitted for double-blind reviewing.

[13] M. D. Mckinley, K. A. Remley, M. Myslinski, J. S. Kenney, D. Schreurs, B. Nauwelaers, EVM calculation for broadband modulated signals, in: ARFTG Microw. Meas. Conf., 2004, pp. 45–52.

[14] K. A. Remley, D. F. Williams, P. D. Hale, C.-M. Wang, J. Jargon, Y. Park, Millimeter-wave modulated-signal and error-vector-magnitude measurement with uncertainty, IEEE Trans. Microw. Theory Techn. 63 (5) (2015) 1710–1720.

[15] P. D. Hale, D. F. Williams, A. Dienstfrey, Waveform metrology: signal measurements in a modulated world, Metrologia 55 (5) (2018) S135.

[16] A. Geens, Y. Rolain, W. Van Moer, K. Vanhoenacker, J. Schoukens, Discussion on fundamental issues of npr measurements, IEEE Trans. Instrum. Meas. 52 (1) (2003) 197–202.

[17] J. B. Sombrin, On the formal identity of evm and npr measurement methods: Conditions for identity of error vector magnitude and noise power ratio, in: Proc. European Microw. Conf., IEEE, 2011, pp. 337–340.

[18] K. Freiberger, H. Enzinger, C. Vogel, A noise power ratio measurement method for accurate estimation of the error vector magnitude, IEEE Trans. Microw. Theory Techn. 65 (5) (2017) 1632–1645.

[19] Y. Rolain, M. Zyari, E. Van Nechel, G. Vandersteen, A measurement-based error-vector-magnitude model to assess non linearity at the system level, in: IEEE MTT-S Int. Microw. Symp., 2017, pp. 1429–1432.

[20] J. Verspecht, A. Stav, J.-P. Teyssier, S. Kusano, Characterizing amplifier modulation distortion using a vector network analyzer, in: ARFTG Microw. Meas. Conf., IEEE, 2019, pp. 1–4.

[21] K. Vanhoenacker, T. Dobrowiecki, J. Schoukens, Design of multisine excitations to characterize the nonlinear distortions during frf-measurements, IEEE Trans. Instrum. Meas. 50 (5) (2001) 1097–1102.

[22] J. C. Pedro, N. B. Carvalho, Designing multisine excitations for nonlinear model testing, IEEE Trans. Microw. Theory Techn. 53 (1) (2005) 45–54.

[23] C. Sanchez-Perez, J. de Mingo, P. Garcia-Ducar, P. L. Carro, A. Valdovinos, Dynamic load modulation with a reconfigurable matching network for efficiency improvement under antenna mismatch, IEEE Trans. Circuits Syst. II Express Briefs 58 (12) (2011) 892–896.

[24] K. Hausmair, S. Gustafsson, C. Sánchez-Pérez, P. N. Landin, U. Gustavsson, T. Eriksson, C. Fager, Prediction of nonlinear distortion in wideband active antenna arrays, IEEE Trans. Microw. Theory Techn. 65 (11) (2017) 4550–4563.

[25] A. M. Angelotti, G. P. Gibiino, A. Santarelli, T. S. Nielsen, J. Verspecht, Combined wideband active load-pull and modulation distortion characterization with a vector network analyzer, in: ARFTG Microw. Meas. Conf., 2021, pp. 1–4.

[26] R. Pintelon, J. Schoukens, FRF measurement of nonlinear systems operating in closed loop, IEEE Trans. Instrum. Meas. 62 (5) (2012) 1334–1345.

[27] Y. Rolain, W. Van Moer, R. Pintelon, J. Schoukens, Experimental characterization of the nonlinear behavior of rf amplifiers, IEEE Trans. Microw. Theory Techn. 54 (8) (2006) 3209–3218.

[28] R. Pintelon, J. Schoukens, System Identification: A Frequency Domain Approach, John Wiley and Sons, 2012.

[29] H. Ochiai, H. Imai, On the distribution of the peak-to-average power ratio in ofdm signals, IEEE Trans. Commun. 49 (2) (2001) 282–289.

[30] 3GPP, Technical Specification Group Radio Access Network 38.104, 38.141 (9 2019).

[31] M. Marchetti, M. J. Pelk, K. Buisman, W. C. E. Neo, M. Spirito, L. C. N. de Vreede, Active harmonic load-pull with realistic wideband communications signals, IEEE Trans. Microw. Theory Techn. 56 (12) (2008) 2979–2988.

[32] A. M. Angelotti, G. P. Gibiino, T. S. Nielsen, D. Schreurs, A. Santarelli, Wideband active load–pull by device output match compensation using a vector network analyzer, IEEE Trans. Microw. Theory Techn. 69 (1) (2020) 874–886.

[33] A. M. Angelotti, G. P. Gibiino, T. S. Nielsen, D. Schreurs, A. Santarelli, Enhanced wideband active load-pull with a vector network analyzer using modulated excitations and device output match compensation, in: IEEE MTT-S Int. Microw. Symp. Dig., 2020, pp. 763–766.

[34] M. Schoukens, J. Hammenecker, A. Cooman, Obtaining the preinverse of a power amplifier using iterative learning control, IEEE Trans. Microw. Theory Techn. 65 (11) (2017) 4266–4273.

[35] A. M. Angelotti, G. P. Gibiino, T. Nielsen, F. F. Tafuri, A. Santarelli, Three port non-linear characterization of power amplifiers under modulated excitations using a vector network analyzer platform, in: IEEE MTT-S Int. Microw. Symp. Dig., 2018, pp. 1021–1024.

[36] Joint Committee for Guides in Metrology, Evaluation of measurement data—guide to the expression of uncertainty in measurement, JCGM 100 (2008) 1–116.